surfaces

MDPI

Article

Modeling the Terminal Velocity of Rising Electrocharged Microbubbles

Roberto Pérez-Garibay [1,*], Arturo Bueno-Tokunaga [2], Francisco Andrés Acosta-González [1] and Ramón Arellano-Piña [3]

[1] Cinvestav IPN, Parque Industrial Saltillo-Ramos Arizpe, Industria Metalúrgica No. 1062, Ramos Arizpe C.P. 25900, Mexico; andres.acosta@cinvestav.edu.mx
[2] Centro de Investigación en Geociencias Aplicadas UAdeC, Calle 5 de Febrero Esquina Blvd. Simón Bolívar # 303-A, Nueva Rosita C.P. 26830, Mexico; arturobueno@uadec.edu.mx
[3] Departamento de Ingeniería Metalúrgica UPIIZ-Zacatecas, Instituto Politécnico Nacional, Zacatecas C.P. 98160, Mexico; larellanop@ipn.mx
* Correspondence: roberto.perez@cinvestav.edu.mx

Abstract: The generation of electrocharged microbubbles is very important for several separation processes (e.g., water treatment, paper industry, and mineral processing). However, their rising terminal velocities are not fully understood. This work presents a laboratory study of the terminal velocity of single microbubbles (bubble diameter (D_b) < 100 μm) rising in stagnant aqueous solutions with different pH levels (from 2 to 12) and reagent types (frother and collector; 30 ppm). The measurements were compared with the respective predicted velocities computed from the Stokes and Hadamard–Rybczynski models. It was found that the terminal velocities of electrocharged microbubbles were larger than the respective predictions from the Stokes equation. A regression equation was proposed to predict the terminal velocity as a function of the bubble diameter, which showed considerable dispersion depending on the type of reagent adsorbed on its surface, the concentration of these reagents, and the physical characteristics that the boundary layer acquires by modifying the zeta potential of the microbubbles; this effect has not yet been addressed in the literature.

Keywords: terminal velocity; zeta potential; microbubbling reactors; microbubbles

Citation: Pérez-Garibay, R.; Bueno-Tokunaga, A.; Acosta-González, F.A.; Arellano-Piña, R. Modeling the Terminal Velocity of Rising Electrocharged Microbubbles. *Surfaces* **2024**, *7*, 979–989. https://doi.org/10.3390/surfaces7040064

Academic Editor: Gaetano Granozzi

Received: 5 September 2024
Revised: 30 October 2024
Accepted: 2 November 2024
Published: 8 November 2024

1. Introduction

The dynamics of small bubbles in all types of bubbling reactors are not fully understood, as explained below. The dynamics of a submerged body in a continuous fluid can be expressed by the following motion equation:

$$\frac{d(m_b v)}{dt} = F_b - F_w - F_k \quad (1)$$

where m_b is the mass of a submerged body moving at velocity v under the action of the following forces: F_b is the buoyant force on the body, F_w is the weight of the body, and F_k is the drag force on the submerged body. This last force can be estimated from different models. The most frequently used approach is given by the Stokes law for a solid sphere moving under laminar flow conditions. The corresponding equation is:

$$F_k = 6\pi R\mu \left| v - v_f \right| \quad (2)$$

where μ is the fluid viscosity, R is the bubble radius, and v_f is the fluid velocity, which is zero for a stagnant medium. The equations above have been applied to the rising of bubbles. In this case, the bubbles accelerate very fast and soon reach a steady rising velocity when $\frac{d(m_b v)}{dt} = 0$. This steady velocity is the so-called terminal velocity (v_t). When the Stokes

drag force is considered, the resultant velocity is termed the Stokes terminal velocity and is given by the following expression:

$$v_{t,ST} = \frac{2gR^2(\rho_f - \rho_b)}{9\mu} \tag{3}$$

where g is the gravity acceleration and ρ_f and ρ_b are the densities of the liquid and the bubble gas, respectively. This velocity has been extensively studied for bubbles having a diameter larger than 100 μm [1–6]. However, corresponding reports for bubbles under 100 μm (microbubbles) are scarce [7–9]. Furthermore, for these latter cases, some information is contradictory. For example, most of the authors agree that experimentally measured velocities are larger than the corresponding terminal velocities predicted by the Stokes model (Equation (3)), but Takahashi [8] reported measured velocity values for bubbles with diameters ranging from 10 to 55 μm that were slightly smaller than those calculated using the Stokes equation. Although these observations could be explained by the differences in how the authors conducted their tests, no clear conclusion could be drawn from their findings. At this point, it is important to note that a bubble is not a solid sphere; although the bubble shape is spherical, internal gas flows by tracking circulatory paths [9]. Therefore, the assumption of a non-slip bubble surface, which is implicit in the Stokes model, is not appropriate for determining the drag force on a bubble. Instead, a bubble is better represented as a fluid sphere with interfacial slip or partial interfacial slip.

Hadamard [10] and Rybczynski [11] proposed, independently of each other, a corrected equation for the Stokes drag force that considers a fluid sphere. The authors measured the settling velocity of spherical droplets submerged in a non-miscible liquid with a different density. The corresponding terminal velocity is known as the Hadamard–Rybczynki ($v_{t(H-R)}$) equation and is expressed as:

$$v_{t(H-R)} = \frac{2gR^2(\rho_f - \rho_b)}{9\mu}\left[\frac{3\mu + 3\mu'}{2\mu + 3\mu'}\right] \tag{4}$$

where μ and μ' are the viscosities of the continuous fluid and the droplets, respectively. It can be shown that this equation is equivalent to Equation (3) when the viscosity of the droplets is much larger than the corresponding value for the continuous liquid, that is, $\mu' \gg \mu$. Of course, this is only valid for solid spheres rather than bubbles. Indeed, the bubble gas viscosity is much smaller than the liquid viscosity, $\mu' \ll \mu$, and Equation (4) becomes the following simplified equation:

$$v_{t(H-R)} = \frac{gR^2(\rho_f - \rho_b)}{3\mu} = \frac{3}{2}v_{t,ST} \tag{5}$$

This means that, for a bubble, the expected terminal velocity is 3/2 times the Stokes terminal velocity. Equation (5) was further validated by Kelsall et al. [12], who reported an agreement between their measured velocities for oxygen bubbles rising in an aqueous solution of 10^{-4} M $NaClO_4$ and the corresponding predictions from this equation. The bubbles were electrolytically generated with diameters in the range of $35 < D_b < 110$ μm. Henry et al. [9] also reported agreement between the measured rising velocities of microbubbles with diameters of $40 < D_b < 100$ μm and the corresponding values computed using Equation (5).

Parkinson et al. [7] studied the velocity of single bubbles of air, nitrogen, helium, and carbon dioxide rising in ultra-clean water. The size and velocity of these bubbles were measured using a high-speed microscopy technique. The bubble diameters were in the range of $10 < D_b < 100$ μm and the authors compared the measured terminal velocities with the corresponding predictions from the Stokes and simplified H–R equations. As expected, they obtained a better mutual agreement with the latter equation. However, their results did not show agreement for carbon dioxide microbubbles, especially for those with a diameter smaller than 60 μm. Their measured terminal velocity was above the value

predicted by Equation (5). The authors ascribed this effect to the enhanced solubility of CO_2 compared with the other gases examined. They inferred that a diffusion boundary layer enriched with CO_2 would form around the bubble. The concentration of this dissolved gas in the region above the bubble should be smaller than the concentration below the bubble. This should promote a surface tension gradient that would drive a larger terminal velocity.

Takahashi [8] determined the zeta potential of air bubbles rising in water at several pH values. They measured the rising velocity component, and the reported values were slightly smaller than those predicted by the Stokes model (Equation (3)). The authors attributed this result to the presence of a hydrogen-bonding network between the bulk water and the gas–water interface. This bonding network behaves as a stagnant liquid surrounding the bubble. Therefore, the slipping surface is a sphere having a radius larger than the bubble radius. This is equivalent to a larger shear area on the bubble that increases the corresponding drag force and leads to a smaller terminal velocity.

It is well known that dissolved salts and surfactants in water modify the surface energy of bubbles generated by a gas blowing into an aqueous solution (providing electrostatic properties to the bubbles). This phenomenon leads to a decrease in the fluid flow velocity within the boundary layer around each bubble. This is equivalent to imposing a non-slip condition on the bubble surface, decreasing the terminal velocity in comparison to a value given by the H–R model [9]. This results in a lower bubble terminal velocity compared to that obtained without the use of surfactants. In fact, when a new bubble is formed, it rises very fast but gradually collects surfactant agents until it reaches a saturation point. This promotes a decrease in the bubble velocity. The period for the bubble to reach a steady velocity is called the aging time.

During the aging time, the zeta potential on the microbubble surface also evolves. Takahashi [8] studied this variable and found, in agreement with other authors, that its value was negative over a wide pH range. Only in acidic solutions of pH < 4 did the zeta potential become positive. Pérez-Garibay et al. [13] reported the effect of electric charge at the surface of microbubbles on the terminal velocity using common chemical reagents for mineral flotation. They showed that the terminal velocity was always larger than the corresponding value computed by the Stokes equation. In summary, the bubble dynamics correspond to those predicted by Equation (5), namely 3/2 times the velocity calculated by the Stokes model. This result is a consequence of the slipping condition at the bubble surface. However, some factors can cause the velocity to deviate from this expected result. Table 1 presents a summary of these factors.

Table 1. Factors that contribute to the deviation of the microbubble dynamics in aqueous solutions from the expected terminal velocity given by Equation (5), according to the literature.

Factor	Reference	Effect on Terminal Velocity	Comments
Presence of surfactant	Navarra et al. [5]	Decreases	Surface tension decreases and bubble surface becomes a non-slipping boundary.
pH in the presence of an electric field	Takahashi [8]	Decreases	A hydrogen-bonding network forms between the bulk water and the gas–water interface, which increases the drag area on the bubble
Dissolved CO_2	Parkinson et al. [7]	Increases for D_b < 60 μm	It may be attributed to the generation of a surface tension gradient due to dissolved CO_2 (Marangoni effect)
Presence of electric charge	Pérez–Garibay et al. [13]	Increases slightly	It may be attributed to double layer physics

The addition of surfactants decreases the surface tension and restores a non-slipping condition to the bubble surface, thereby decreasing the rising velocity to a value predicted by the Stokes model. Another source which decreases the terminal velocity is the presence of a hydrogen-bonding network between the bulk water and the gas–water interface. This acts as a stagnant region that promotes a larger drag force on the bubble. The factors proposed to explain an increase in the terminal velocity are also shown in the table. These factors seem to affect only very small bubbles, with D_b < 60 μm, and the reasons are not clear. This work reports a study of laboratory measurements of terminal velocities for air electrocharged microbubbles rising in aqueous solutions at several pH values and with different types of chemical reagents (frother and collector), which are commonly used to change the superficial charge of the bubbles.

2. Materials and Methods

2.1. Bubble Zeta Potential Measurements

It is opportune to mention that the bubble zeta potential data presented in this work and the experimental methodology were described elsewhere in the literature and the reader can consult it for more information [13,14]. However, a summary is included for convenience and to facilitate the understanding of this work. The setup contained three major components: a high-pressure air saturation container, the electrophoretic cell, and the image acquisition system. The bubbling cell was an atmospheric reservoir (30 cm height, 10 cm length, and 15 cm width) that was fabricated out of transparent acrylic plaques.

The video camera was focused on the electrophoretic cell (for more detail consult Bueno-Tokunaga [14]). The laboratory configuration cell was as illustrated in Figure 1 for the terminal velocity measurements. An important element of the experimental setup was the image acquisition system, which was composed of a digital camera equipped with a macro lens (Navitar® 12×, Rochester, NY, USA). The video camera (Toshiba 3-CCD RGB; resolution 1024 × 768 pixels; 90 frames/s) permitted the user to register the bubble displacement and the time through a MATLAB® library that linked the video camera to the computer. Each image was recorded in a file whose name included the time at which the image was taken. The bubble velocity was estimated from the recorded images by dividing the bubble displacement by the corresponding time.

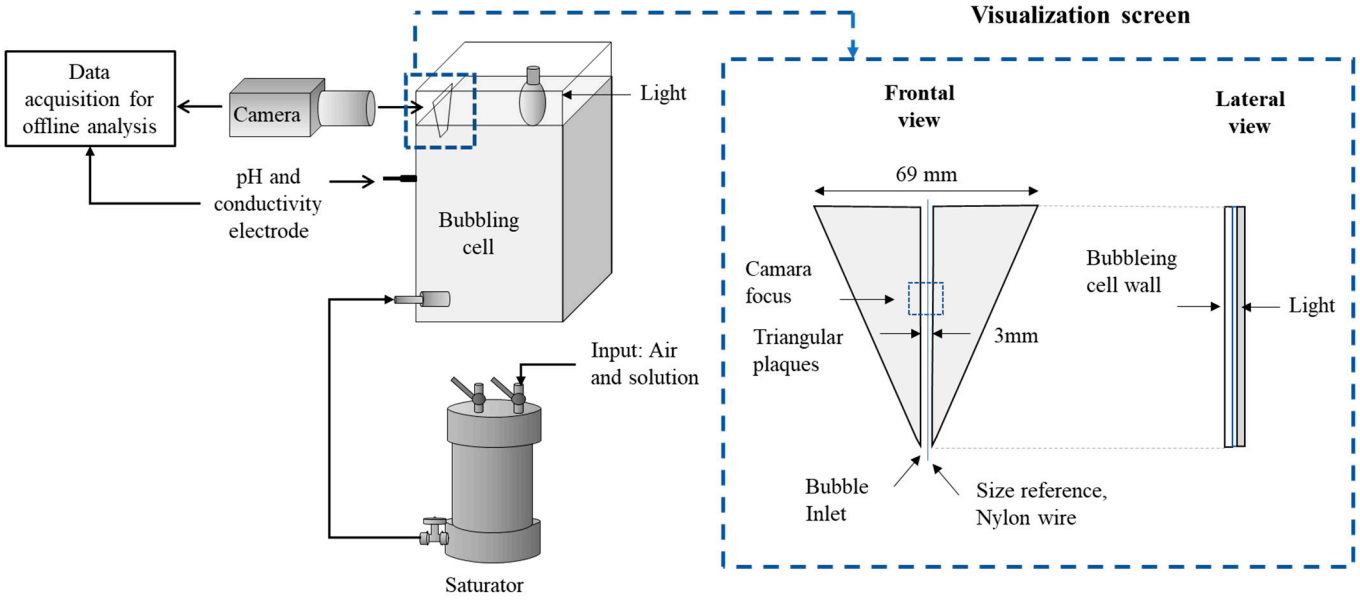

Figure 1. Schematic representation of the laboratory setup for terminal velocity measurements.

The first requirement to obtain reliable images was the visualization of a single microbubble rising close to the reference object (Nylon wire 230 μm diameter, Wuhan, China).

Once the aqueous solution (3.5 L) was prepared, the pH, electrical conductivity, and temperature (25 °C) were recorded. To provide a controlled electric strength, enough NaCl was added to the aqueous solution to reach a concentration of 10^{-3} M. This aqueous solution was agitated for 5 min to stabilize the temperature and to homogenize the solution after the reagent addition. The solution was fed into the electrophoretic cell and into the closed tank which was thereafter pressurized at 690 kPa (100 psi) of air. To initiate bubble formation, the valve located at the output of the saturator tank was opened (instantaneous pulse), introducing the saturated solution at ~8 cm horizontal distance and 19 cm below from the visualization screen (see Figure 1). At the beginning of each test, approximately 1 cm^3 of aqueous solution with dissolved air was added to 3000 cm^3 of stagnant water. It was evident that this injection did not change the terminal velocity of the microbubble for the following reason: after the little increase in volume (from 3000 to 3001 cm^3) many seconds passed (400 s, assuming a velocity of 0.500 m/s) before the bubbles reached the visualization screen (19 cm above) and after 400 s the bubbling cell was completely stagnant.

2.2. Terminal Velocity Measurements

Microbubbles were formed from an air-supersaturated aqueous solution at a manometric air pressure of 690 kPa (100 psi). Then, a jet of supersaturated solution flowed out briefly to the bubbling cell, of 4 L capacity, and the depressurized solution released a swarm of microbubbles in the water saturated with air under atmospheric conditions. Special attention was made to avoid temperature gradients within the bubbling cell to prevent the natural convection of the liquid and consequently the uncontrolled microbubble rising; to achieve this goal the temperature of the aqueous solution and the laboratory atmosphere were homogenized at 25 °C. Another possible source of liquid convection that was avoided was the high airflow stream over the surface of the aqueous solution.

To reduce the number of bubbles entering the visualization screen, this screen was placed on a cell wall, far away from the input of the supersaturated solution, as shown in Figure 1. This also ensured that terminal velocity was reached. This zone was in fact a vertical transparent channel which screened solitary bubbles for observation.

For this experimental set, collector and frother reagents that were investigated were as follows: (a) potassium ethyl xanthate ($C_3H_5KOS_2$, 96%; Sigma-Aldrich, St. Louis, MO, USA), (b) dodecylamine ($C_{12}H_{27}N$, 98%; Sigma-Aldrich), (c) terpineol ($C_{10}H_{18}O$, 98%; Sigma-Aldrich), and (d) methyl-isobutyl-carbinol (MIBC, 98%; Sigma-Aldrich). Their concentrations are shown in Table 2. These solutions had a controlled ionic force using 10^{-3} M NaCl. Electrical conductivity, pH, and temperature were also registered. Surface tension (γ) was also measured for most of the studied solutions with a surface tensiometer (model 20, Fisher Scientific®, Hampton, NH, USA). The surface tension behavior has been observed by Castro et al. [15] and Pérez-Garibay et al. [13], who mentioned that the combination of salts and surfactants can generate complex effects.

Table 2. Collector and frother concentrations used in this work. Surface tension values appear in square brackets after the respective pH values.

Chemical Reactive	Concentration, ppm	pH [γ(dyn/cm)]
Xanthate	30	2.4 [59], 4.3 [64], 6.2 [66], 8.13 [66], 10.06 [59], 12 [56]
Dodecylamine	30	2.47 [38.76], 3.46 [41.93], 5.24 [48.27], 7.05 [50.54], 9.50 [45.55], 11.44 [37.85]
MIBC	7, 10, 30	2.98 [52.58], 5.21 [54.38], 7.23 [55.28], 9.54 [54.83], 11.55 [53.93]
Terpineol	25	2.18 [48.92], 3.44 [54.87], 8.75 [53.72], 10.34 [52.95], 12.10 [52.38]

It is important to mention that previous work by Pérez-Garibay et al. [13] proved that the microbubble terminal velocity was measured correctly, and showed that the rising bubble velocity was kept constant in the visualization zone. The bubbles had traveled a distance equivalent to 2600 times their bubble diameter from the input port to the visualization screen.

2.2.1. Image Recording for Measuring Bubble Diameter and Terminal Velocity

Images were displayed on the monitor, which had superimposed a millimetric grid previously prepared to assign units to the reference diameter wire (230 µm), as shown in Figure 2. Based on this grid, the length scale of the amplified bubble image was determined, and then the actual size of the bubble was determined from a direct proportion. This procedure was also used to estimate the actual displacement of the bubble. For each pH of the aqueous solutions, sequences of ten tests with 200 photos each were performed. Then, the diameter of the bubbles was estimated, and the velocity of the bubble was determined.

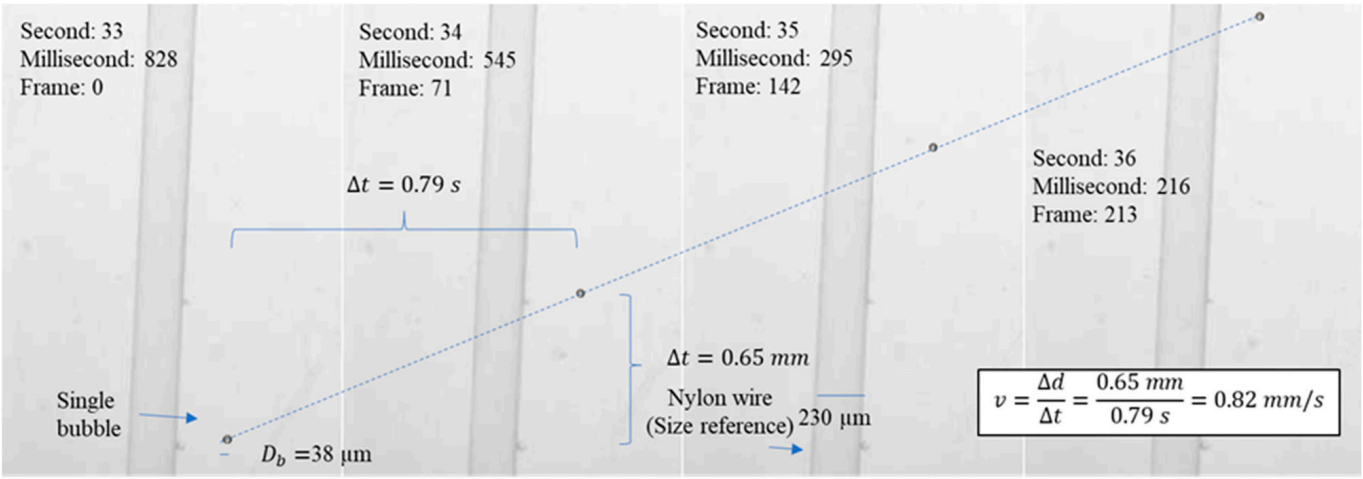

Figure 2. Sequential photographs of a rising bubble and reference wire.

2.2.2. Standard Deviation of Terminal Velocity Data and Bubble Diameter Absolute Error

Regarding the bubble diameter error, it is worth mentioning that, due to the movement of the bubbles and the millimeter grid size superposed on the monitor, the estimation of the diameter with this technique involved an absolute error of ~4.6 µm (this error is because the edge of the microbubbles is diffuse, but it has an insignificant effect on the terminal velocity estimation). It is also relevant to say that experimental errors were always normally distributed with a mean equivalent to the value represented by the tendency curves, which confirms the reliability of the results.

It is important to note that the values of terminal velocity and their dispersion which were observed in this work are consistent with those reported in the literature [7,8,12]. This reinforces the certainty of our results.

3. Results

The measured single air bubble velocities were compared with the respective predictions from the Stokes equation. Figure 3a–d show this comparison when using frother (MIBC and terpineol) and collector agents (xanthate and dodecylamine) which change the superficial charge of the bubbles, at several concentrations and pH values.

The straight line indicates a perfect agreement between them. Points located below this line correspond to cases where the measured velocity was larger than the respective prediction; therefore, practically all measured velocities were larger than the Stokes terminal velocities. Terpineol and xanthate showed a smaller deviation from Stokes law when compared with MIBC and dodecylamine. This last case presented the highest measured velocities.

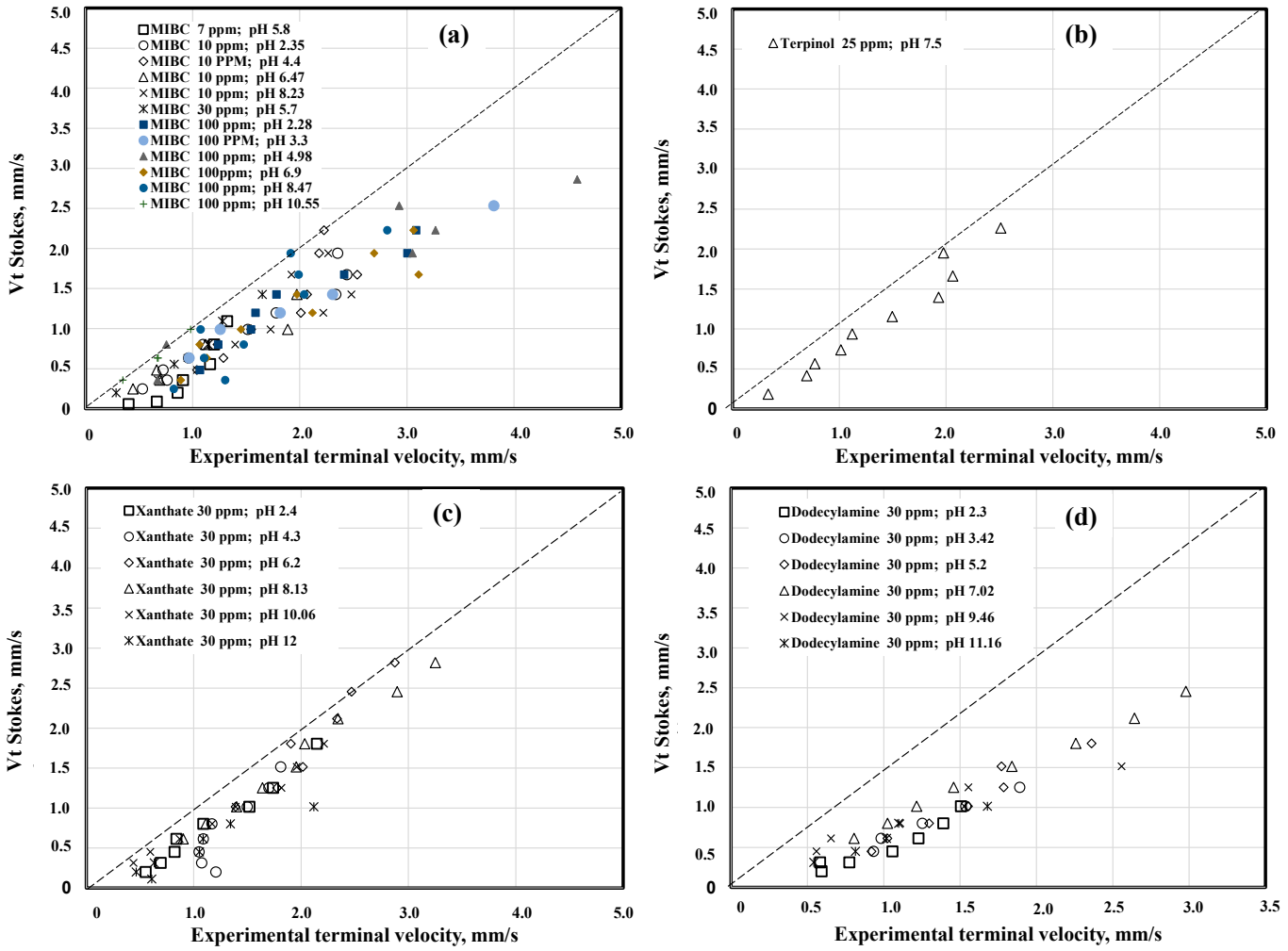

Figure 3. Comparison between the measured terminal velocity and the corresponding Stokes velocity for single air bubbles rising in aqueous solutions containing: (**a**) MIBC, (**b**) terpineol, (**c**) xanthate, and (**d**) dodecylamine at the indicated concentrations and pH values.

Figure 4a–c present comparisons of the measured values with those calculated by the Stokes law, the H–R model, and a regression equation derived from the present work using all the previous data, respectively. The H–R model describes the terminal velocity better than the Stokes equation does. Nevertheless, the smaller bubbles rose at a higher velocity than predicted by the H–R equation. Larger bubbles seemed to be less prone to this behaviour. The regression equation that corresponds to the experimental data is:

$$v_t = 1.334 v_{t,ST} \quad (6)$$

This equation corresponds to the straight line that is drawn in Figure 4c and represents an empirical relationship between the measured velocity, vt, and the corresponding Stokes prediction. The regression coefficient (R^2) was 0.81, which indicated some degree of data dispersion. The experimental data of this figure include the information obtained with different chemical conditioning reagents. As observed in Figure 3, with each chemical conditioning a trend with less dispersion was obtained, but when all the trends were represented in a single graph, the greatest dispersion was observed.

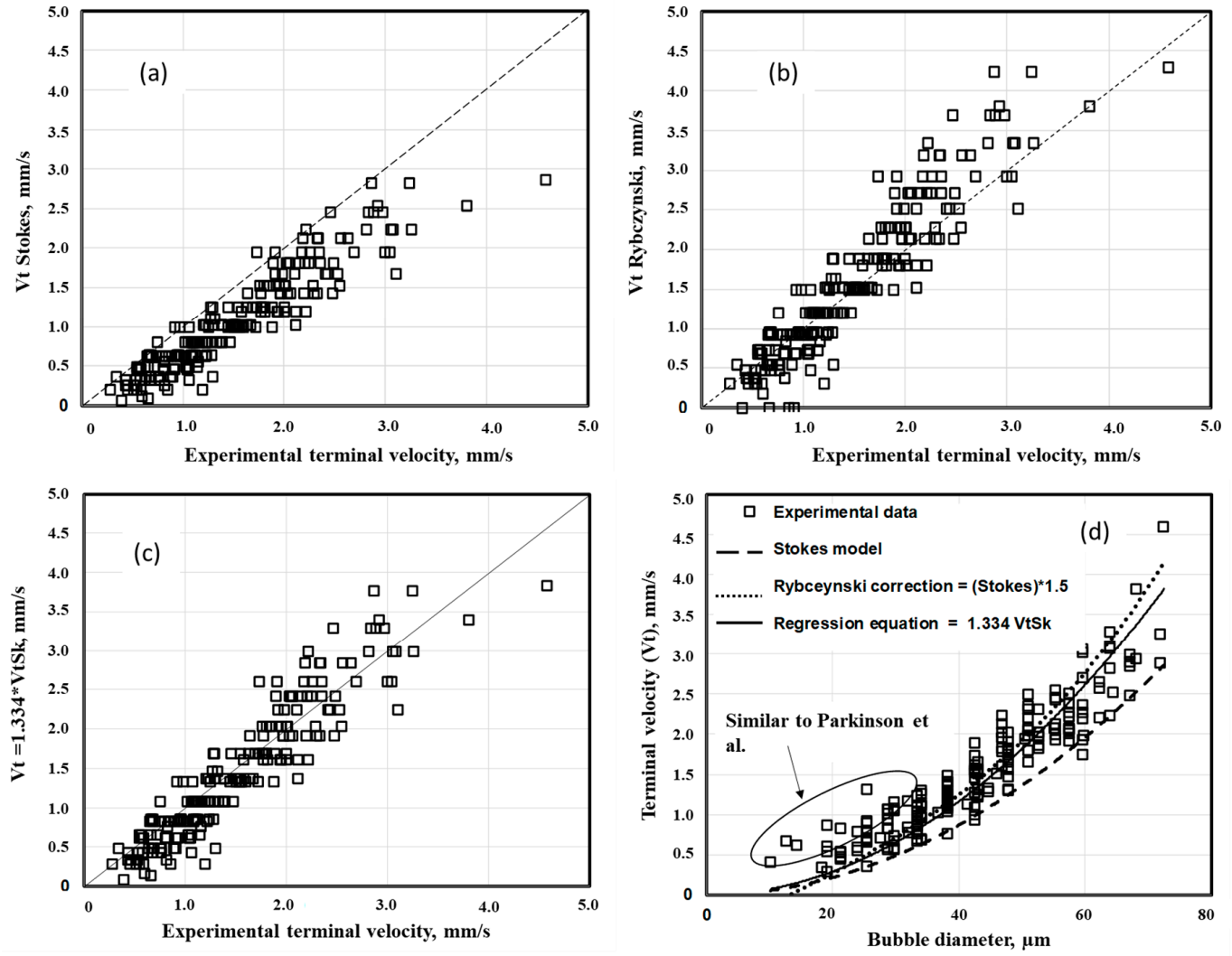

Figure 4. Comparison between the measured terminal velocities of single air bubbles in aqueous solutions with foaming agents added as collectors and the corresponding predictions from (**a**) Stokes law, (**b**) the Hadamard–Rybczynski model, (**c**) the regression equation from the present work, and (**d**) plot of the terminal velocity versus bubble diameter (similar deviations were obtained by Parkinson et al. [7]).

It is worth mentioning that a total of 210 average velocities were used to obtain this regression equation. Also, each average velocity was determined from 20 velocity measurements using bubbles with similar diameters. The measured terminal velocity was 1.334 larger than the expected Stokes value. However, it was smaller than the value predicted by the H–R model for air bubbles rising in pure water.

Another point of view regarding these results is shown in Figure 4d, where the terminal velocity is plotted versus bubble diameter. The experimental data were located between the Stokes and H–R models, and the regression equation provided the best result. Each experimental point in Figures 3 and 4 represents the average of the diameter and experimental terminal velocity of a closed class of microbubble sizes, composed of 30 measurements. Because it would take up a lot of space to show the statistics of each point, as an example it is mentioned that for an average diameter of 58.6 µm, the standard deviation was 0.77 µm.

4. Discussion

These results were obtained under the controlled conditions of temperature, aqueous solution composition, and laminar dynamics. However, real industrial conditions generally have temperature gradients, turbulent dynamics, and hindered flotation (many

bubbles). Under these less controlled conditions it is possible that the terminal velocity of the microbubbles is mainly governed by the convective movements of the continuous phase (generally water).

To analyze these results, it is important to realize that rising microbubbles have low Reynolds numbers, <1, which would lead to a fore–aft symmetry in the concentration contours of the microbubble. Microbubbles rise at relatively low velocities; therefore, the diffusion layer of ions is expected to be distributed uniformly around each microbubble, possibly generating a low bubble polarization. Another aspect to discuss about the results of Figure 4d is that for each microbubble diameter there is a significant dispersion of terminal velocities which can be thought of as being due to the standard deviation of the velocity measurements. However, this deviation does not explain all the dispersion for these results. At this point it is important to mention that it has already been recognized by some researchers [16,17] that bubbles of the same diameter may have different terminal velocities when their surface is conditioned with different surfactant reagents. That allows us to ensure that the apparent dispersion of Figure 4d is also determined by the physical chemistry of the bubble surface. In previous work, Pérez–Garibay et al. [13] observed that even by conditioning the surface of the bubbles with the same surfactant and under the same concentration, the terminal velocity of the microbubbles can vary according to the electric charge intensity at their surface. For example, Figure 5 shows the zeta potential effect on terminal velocities being observed with both the cationic (dodecylamine) and the anionic (xanthate) surfactants. The result was a slight increase in velocity, with a more pronounced effect with small bubbles and cationic collectors. We also noted that, using the cationic surfactant the microbubbles increased their velocity at an acidic pH, while using an anionic surfactant such as xanthate the bubbles increased their velocity at an alkaline pH. This behavior was explained previously as follows [13]: in the case of xanthate, the decomposition products are hydrolyzed in the solution (xanthate, trithiocarbonate, xanthic acid, xanthic acid compound, dixanthogen, perxanthate, monothiocarbonate, dithiocarbonate, and sulfide), and all these products act as weak bases, competing with each other to take a space at the bubble interphase and contributing to a low and negative electrical charge at the bubble surface; in the case where the microbubbles are conditioned with dodecylamine at an alkaline pH, the hydroxyl anions adsorbed on the bubble attract the cations of the collector, increasing the boundary layer thickness and decreasing its terminal velocities. It is opportune to mention that, although the effect of the electric charge and the double electric layer was more noticeable with a strong polar surfactant (dodecylamine) than with xanthate; with the frother agents this effect was less notorious, and its behavior was almost similar to that of the bubbles in deionized water. Additionally, it could be thought that it is the change of surface tension, through the effect of pH, which is responsible for the terminal velocity changes; but, if this were so, this speed would change parabolically as shown by Bueno-Tokunaga et al. [14], but this does not happen with the zeta potential effect.

Another interesting observation about Figure 4d is that the H–R model underestimated the measured velocity for bubbles that were smaller than 30 μm, while it seemed to overestimate most of the velocities for bubbles larger than 60 μm. This latter result can be explained by considering the decrease in velocity due to the added surfactants, as explained in Table 1. However, a velocity increase for the smallest bubbles cannot be explained by the classic dynamics of submerged spheres.

The only known work to report a high velocity for microbubbles is Parkinson et al. [7] when using CO_2 bubbles with a diameter smaller than 40 μm. In this case, the authors elaborated an explanation based on CO_2 solubility in water, as explained in Section 1. In our case, it is proposed that the experimental methodology used to generate the smallest bubbles involved very acidic or very alkaline pH conditions and high concentrations of reagents, which could have influenced the generation of invisible nano-bubbles and altered the terminal velocity of smaller microbubbles. To elucidate if the same phenomena occurs without nano-bubbles, it is suggested that in future research the microbubbles are generated by a different method than from dissolved air, because this one involves the formation of nano-bubbles.

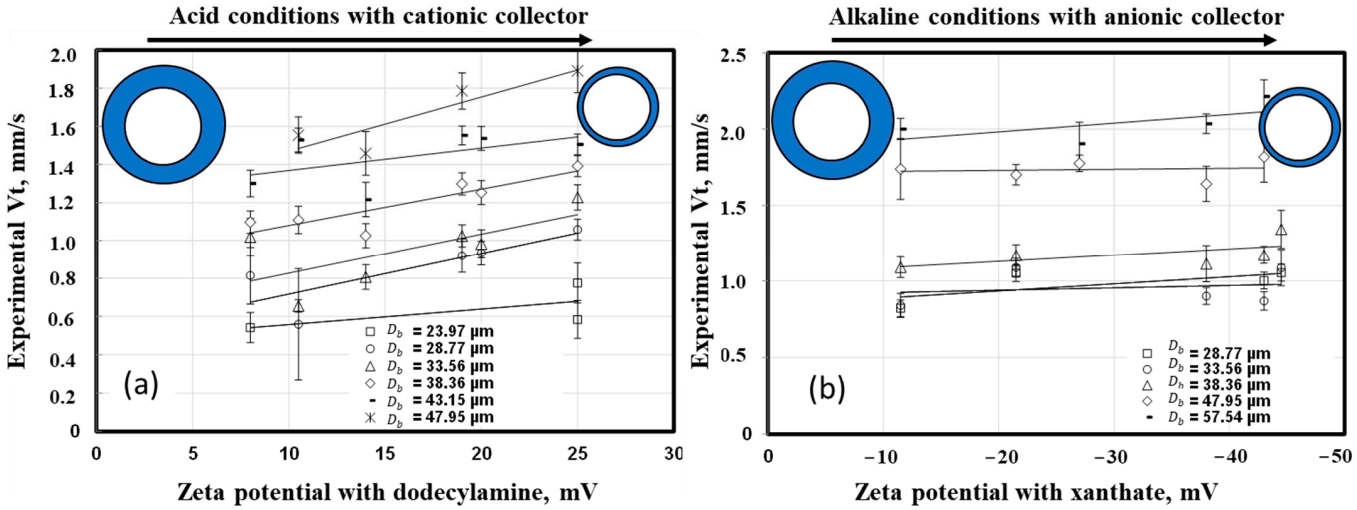

Figure 5. Effect of zeta potential on the terminal velocity of microbubbles. (**a**) Conditioned with 100 ppm of dodecylamine and different pH. (**b**) Conditioned with 30 ppm of xanthate and different pH.

5. Conclusions

This work is an experimental study of the terminal velocity of single air microbubbles rising in aqueous solutions with surfactants used for the mineral flotation process under a wide range of concentrations. Bubbles up to 100 µm in diameter were generated from high-pressure air supersaturated solutions which were fed to a tank under atmospheric pressure.

From the current knowledge of single bubble dynamics, it was expected that the measured terminal velocities would follow Stokes predictions because the surface tension decreased with surfactants and pH. However, the measured velocities were always larger than the corresponding predictions based on the Stokes model.

The measured rising velocities were correlated with the Stokes terminal velocity and the resulting regression equation showed a slope value of 1.334 rather than the value of 1.5 predicted by the Hadamard–Rybczynski model.

It was observed that for each microbubble diameter there was a significant dispersion of terminal velocities, which was in agreement with Azgomi et al. [16] and Rafiei et al. [17], explaining that this is possible when bubbles of the same diameter are conditioned with different surfactant reagents. This can also be influenced by the physical chemistry and electric double layer of the bubble surface. The presence of nano-bubbles around the microbubbles would have an influence in decreasing the drag coefficient. This would lead to an increase in the terminal velocity.

Even when the technology used in this study is enough to generate meaningful measurements of microbubble diameters and terminal velocities, it is desirable to increase the number of pixels per unit area of the lens to decrease the diameter measurement uncertainty. Similarly, the uncertainties in the experimental velocities could be lowered if the camera could take photographs at a higher speed. Since it is not easy to obtain simultaneously a maximum bubble resolution and a high video camera speed, it is suggested that the experimental setup be modified. A single camera of high-resolution would measure the bubble diameter, and a second camera would estimate the terminal velocity.

Author Contributions: Conceptualization and methodology, R.P.-G. and A.B.-T.; software, F.A.A.-G.; investigation, A.B.-T.; resources and data curation, R.A.-P.; writing—original draft preparation, R.P.-G. and F.A.A.-G.; writing—review and editing, R.A.-P.; supervision, R.P.-G.; and project administration and funding acquisition, F.A.A.-G. All authors have read and agreed to the published version of the manuscript.

Funding: This study was also funded by Cinvestav-IPN internal projects (1068, 1131).

Institutional Review Board Statement: Not applicable.

Informed Consent Statement: Not applicable.

Data Availability Statement: Experimental data will be available upon personal request.

Acknowledgments: The authors are grateful to CONACYT for funding and to Carmelita Yamamoto Chavarria for assistance with the data collection.

Conflicts of Interest: The authors declare no conflict of interest.

References

1. Talaia, M.A. Terminal velocity of a bubble rise in a liquid column. *World Acad. Sci. Eng. Technol.* **2007**, *28*, 264–268.
2. Bozzano, G.; Dente, M. Shape and terminal velocity of single bubble motion: A novel approach. *Comput. Chem. Eng.* **2001**, *25*, 571–576. [CrossRef]
3. Del Castillo, L.A.; Ohnishi, S.; White, L.R.; Carnie, S.L.; Horn, R.G. Effect of disjoining pressure on terminal velocity of a bubble sliding along an inclined wall. *J. Colloid Interface Sci.* **2011**, *364*, 505–511. [CrossRef] [PubMed]
4. Hayashi, K.; Tomiyama, A. Effects of surfactant on terminal velocity of a Taylor bubble in a vertical pipe. *Int. J. Multiph. Flow* **2012**, *39*, 78–87. [CrossRef]
5. Navarra, A.; Acuña, C.; Finch, J.A. Impact of frother on the terminal velocity of small bubbles. *Int. J. Miner. Process.* **2009**, *91*, 68–73. [CrossRef]
6. Tomiyama, A.; Celata, G.P.; Hosokawa, S.; Yoshida, S. Terminal velocity of single bubbles in surface tension force dominant regime. *Int. J. Multiph. Flow* **2002**, *28*, 1497–1519. [CrossRef]
7. Parkinson, L.; Sedev, R.; Fornasiero, D.; Ralston, J. The terminal rise velocity of 10–100 μm diameter bubbles in water. *J. Colloid Interface Sci.* **2008**, *322*, 168–172. [CrossRef] [PubMed]
8. Takahashi, M. Zeta Potential of Microbubbles in Aqueous Solutions: Electrical Properties of the Gas−Water Interface. *J. Phys. Chem. B* **2005**, *109*, 21858–21864. [CrossRef] [PubMed]
9. Henry, C.L.; Parkinson, L.; Ralston, J.R.; Craig, V.S.J. A Mobile Gas-Water Interface in Electrolyte Solutions. *J. Phys. Chem. C* **2008**, *112*, 15094–15097. [CrossRef]
10. Hadamard, J. Mouvement permanent lent d'une sphère liquide et visqueuse dans un liquide visqueux. *CR Acad. Sci* **1911**, *152*, 1735–1738.
11. Rybczynski, W. On the translatory motion of a fluid sphere in a viscous medium. *Bull. Acad. Sci. Crac. Ser. A* **1911**, *40*, 073605-18.
12. Kelsall, G.H.; Tang, S.; Yurdakul, S.; Smith, A.L. Electrophoretic behaviour of bubbles in aqueous electrolytes. *J. Chem. Soc. Faraday Trans.* **1996**, *92*, 3887–3893. [CrossRef]
13. Pérez-Garibay, R.; Bueno-Tokunaga, A.; Estrada-Ruiz, R.H.; Camacho-Ortegón, L.F. Effect of surface electrical charge on microbubbles' terminal velocity and gas holdup. *Miner. Eng.* **2018**, *119*, 166–172. [CrossRef]
14. Bueno-Tokunaga, A.; Pérez-Garibay, R.; Martínez-Carrillo, D. Zeta potential of air bubbles conditioned with typical froth flotation reagents. *Int. J. Miner. Process.* **2015**, *140*, 50–57. [CrossRef]
15. Castro, S.; Miranda, C.; Toledo, P.; Laskowski, J.S. Effect of frothers on bubble coalescence and foaming in electrolyte solutions and seawater. *Int. J. Miner. Process.* **2013**, *124*, 8–14. [CrossRef]
16. Azgomi, F.; Gomez, C.O.; Finch, J.A. Correspondence of gas holdup and bubble size in presence of different frothers. *Int. J. Miner. Process* **2007**, *83*, 1–11. [CrossRef]
17. Rafiei, A.A.; Robbertze, M.; Finch, J.A. Gas holdup and single bubble velocity profile. *Int. J. Miner. Process.* **2011**, *98*, 89–93. [CrossRef]